iScience

CellPress
OPEN ACCESS

Article

Phototransduction in a marine sponge provides insights into the origin of animal vision

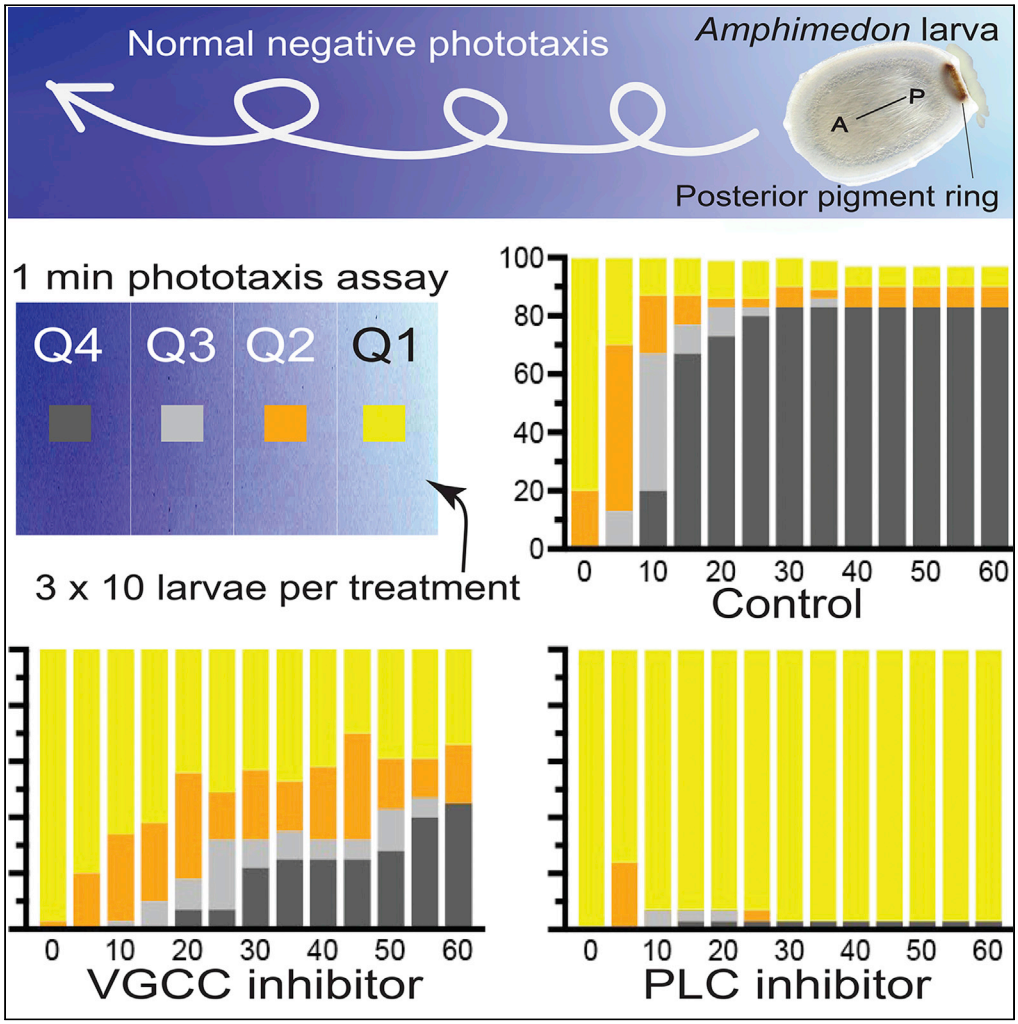

Eunice Wong, Victor Anggono, Stephen R. Williams, Sandie M. Degnan, Bernard M. Degnan

b.degnan@uq.edu.au

Highlights

Amphimedon larvae are negatively phototactic but lack neurons and opsins

Sponge larval photosensory cells are enriched in conserved phototransduction genes

Conserved photosignaling pathways appear to be controlling larval phototaxis

Phototactic behavior is reversed by the inhibition of phospholipase-C

Wong et al., iScience *25*, 104436
June 17, 2022
https://doi.org/10.1016/j.isci.2022.104436

iScience

CellPress
OPEN ACCESS

Article

Phototransduction in a marine sponge provides insights into the origin of animal vision

Eunice Wong,[1] Victor Anggono,[2,3] Stephen R. Williams,[2] Sandie M. Degnan,[1] and Bernard M. Degnan[1,4,*]

SUMMARY

Most organisms respond to light. Here, we investigate the origin of metazoan phototransduction by comparing well-characterized opsin-based photosystems in neural animals with those in the sponge *Amphimedon queenslandica*. Although sponges lack neurons and opsins, they can respond rapidly to light. In *Amphimedon* larvae, this is guided by the light-sensing posterior pigment ring. We first use cell-type-specific transcriptomes to reveal that genes that characterize eumetazoan Gt- and Go-mediated photosystems are enriched in the pigment ring. We then apply a suite of signaling pathway agonists and antagonists to swimming larvae exposed to directional light. These experiments implicate metabotropic glutamate receptors, phospholipase-C, protein kinase C, and voltage-gated calcium channels in larval phototaxis; the inhibition of phospholipase-C, a key transducer of the Gq-mediated pathway, completely reverses phototactic behavior. Together, these results are consistent with aneural sponges sharing with neural metazoans an ancestral set of photosignaling pathways.

INTRODUCTION

Photosensory behavior and phototransduction have been widely studied in bilaterian animals, most comprehensively in mammals, insects, and molluscs (Dorlöchter and Stieve, 1997; Fain et al., 2010; Fein and Cavar, 2000; Feuda et al., 2014; Koyanagi et al., 2008; Lamb, 2013; Montell, 2012; Oakley and Speiser, 2015; Rayer et al., 1990; von Salvini-Plawen, 2008). All neural metazoans (ctenophores, cnidarians, and bilaterians) appear to use a photoreception and signaling system based on opsin, a functionally diverse group of G-protein-coupled receptors (GPCRs) (Feuda et al., 2012; Oakley and Pankey, 2008; Plachetzki et al., 2010; Shichida and Matsuyama, 2009). Rhabdomeric opsins (r-opsins), best known in fly photoreceptors, bind Gα-q protein to activate the phospholipase-C (PLC) pathway that opens transient receptor potential (TRP) channels to depolarize the cell (Montell, 2012; Ranganathan et al., 1991). Ciliary opsins (c-opsins) target multiple types of Gα proteins and thereby activate different cascades that result in cell hyperpolarization. When bound to the vertebrate-only Gα-t protein, it activates phosphodiesterase (PDE) to close cyclic nucleotide-gated (CNG) channels (Lamb, 2013; Oakley and Pankey, 2008; Rayer et al., 1990). Recent revisions consider a third group, RGR/Go-opsins, a sister lineage of c-opsins which transduce through similar cell-hyperpolarizing pathways mediated by the second messenger cyclic guanosine monophosphate (cGMP) (del Pilar Gomez and Nasi, 1998; Feuda et al., 2014, 2012). The diversity of animal opsins, though appreciably large, is likely yet underestimated (Oakley and Speiser, 2015; Ramirez et al., 2016).

Opsin-mediated photosignaling can alter membrane potentials to evoke rapid electrical signal propagation and effective intercellular signaling (del Pilar Gomez and Nasi, 1998; Rayer et al., 1990). This photosystem has been proposed to have evolved from a simple bi-cellular "prototype eye" that was capable of directional light sensing by using fundamentally a shading pigment in the vicinity of a photoreceptor and motile cilia (Arendt and Wittbrodt, 2001; Gehring, 2014; Jékély, 2009). More complex eyes subsequently evolved through the functional segregation of the pigment-photoreceptor and the motile cilium, and the evolution of interconnecting axons that enhance the signal transduction (Arendt et al., 2009).

Sponges are the oldest phyletic lineage of animals without both neurons and opsin genes (Ellwanger and Nickel, 2006; Renard et al., 2009; Rivera et al., 2012; Srivastava et al., 2010). Despite lacking neural eyes, sponges are capable of directional light sensing using photosensory pigment cells and motile cilia (Elliott et al., 2004; Leys and Degnan, 2001; Maldonado et al., 2003). This suggests the metazoan ancestor minimally used this combination of functional components to directionally respond to light. Larvae of the

[1]School of Biological Sciences, University of Queensland, Brisbane, QLD 4072, Australia

[2]Queensland Brain Institute, University of Queensland, Brisbane, QLD 4072, Australia

[3]Clem Jones Centre for Ageing Dementia Research, University of Queensland, Brisbane, QLD 4072, Australia

[4]Lead contact

*Correspondence: b.degnan@uq.edu.au

https://doi.org/10.1016/j.isci.2022.104436

sponge *Amphimedon queenslandica* have a photosensory system comprising a radially symmetrical ring of cells at the posterior end that have either (i) pigmented cellular projections, (ii) long motile cilia, or (iii) a combination of both (Leys et al., 2002; Leys and Degnan, 2001). This posterior ring of shade and receptor cells generates a stereotypic negative phototactic behavior in the swimming larva without the need for neuronal signals (Leys and Degnan, 2001). Other sponge larvae have similar systems (Elliott et al., 2004; Maldonado et al., 2003). Cryptochrome (CRY), a blue-light receptive flavoprotein known to mediate circadian rhythms in bilaterians (Cashmore et al., 1999; Michael et al., 2017), is expressed in these larval photosensory cells (Rivera et al., 2012), suggesting that it plays a photoreceptor role instead of opsin. CRY also appears to be involved in light-dependent diurnal rhythms in *Amphimedon* (Jindrich et al., 2017).

Here, we combine cell type transcriptome analyses with phototaxis assays in larvae exposed to agonists and antagonists of opsin-mediated pathways to determine if the aneural photosystem in *Amphimedon* larvae functions similarly to the opsin-based photosensory systems in neural animals. We find that larval pigment ring cells are enriched in genes encoding Gt- and Go-mediated signal transduction pathways. The impacts of their agonists and antagonists on larval phototaxis appear conserved between sponges and neural metazoans, suggesting GPCR signaling pathways that orchestrate animal phototransduction have been conserved since the metazoan ancestor.

RESULTS

Larval cell type transcriptomes reveal that pigment ring cells express conserved phototransduction genes

We mechanically dissociated swimming *Amphimedon* larvae at 2–3 h post-emergence (hpe) into cells and enriched cell clumps, and then manually isolated seven cell types and populations based on cell shape and size, differential dye uptake, and fluorescence. The seven cell types were cells of the posterior pigment ring, epithelial cells, flask cells, globular cells, cells of the inner cell mass (ICM), sclerocytes, and cuboidal cells (Figure 1). Cell type isolations were repeated multiple times on different cohorts of larvae (Table S1). In all cases, cells were snap frozen within 30 min of dissociation to minimize transcriptional changes.

Transcripts in these pools of cells were sequenced using CEL-Seq2 (Hashimshony et al., 2016) and reads were mapped to Aqu2.1 gene models (Fernandez-Valverde et al., 2015). After quality filtering, 24 transcriptomes representing all cell enrichments, except cuboidal cells which did not retain enough replicates (Table S1; see STAR Methods), were used in subsequent analyses (Figure 1). Principle component analysis reveals an overlap between transcriptomes. The ICM, which has a mixture of cell types including pluripotent archaeocytes and globular cells, has the most overlap with other cell types; globular cells are also present on the larval surface (Figure 1H).

We first sought to determine if 840 *Amphimedon* orthologs of genes with known neural roles in other animals, including synaptic genes (Wong et al., 2019); Table S2) are enriched in any of these cell populations. Comparison of gene expression profiles using DESeq2 reveals that these neural genes are significantly upregulated in the ICM ($p < 0.001$), downregulated in pigment ring cells ($p = 0.014$), and both up- and downregulated in epithelial cells ($p = 0.043$ and $p < 0.001$, respectively) (Figure 2A and 2B).

Although pigment ring cells are not enriched in neural orthologs, genes involved in signal transduction are significantly upregulated in these cells compared to all other larval cell types (Figure 2C and S1). These include adenylate cyclase (AC), phosphodiesterases (PDE), and atrial natriuretic peptide receptor (NPR), which is linked to guanylyl cyclase (GC) (Figure 2D). These enzymes and receptors, although each likely to have multiple roles in signaling, share a common involvement in opsin-driven phototransduction processes (del Pilar Gomez and Nasi, 2000; Luo et al., 2010; Yarfitz and Hurleys, 1994) and their upregulation in pigment ring cells is consistent with a role in regulating photosensory behavior in larvae. The upregulation of calcium/calmodulin-regulated receptor-like kinase (CRLK) further suggests the involvement of calcium in modulating this photosignaling activity. Supporting these results is a significant enrichment of transcripts encoding protein kinase domain-containing proteins in these cells (Table S2), an attribute shared with *Amphimedon* neural genes (Figure S2).

We then specifically selected a suite of genes for their potential roles in photoreception, including orthologous gene families encoding components of bilaterian phototransduction systems, and compared their cell-type-specific expressions. This included all sponge paralogs within an orthologous group and

A

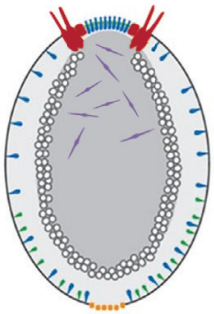

Cell type / population	Identifying features when dissociated
Pigment cells (P)	Clumps of dark brown cells (plate C)
Inner cell mass (I)	Clumps of mixed cell types from larval centre
Epithelial cells (E)	Sheets of small cells with short cilia
Globular cells (G)	Red/green fluorescence when exposed to 2μM NR >10 min (plate D)
Flask cells (F)	Red fluorescence when exposed to 1μM CM-DiI >30 min (plate E)
Sclerocytes (S)	Elongate cells with spicule (plate C)
Cuboidal cells (C)	Bright red when exposed to 10μM NR >30 min (plate F, G)

B

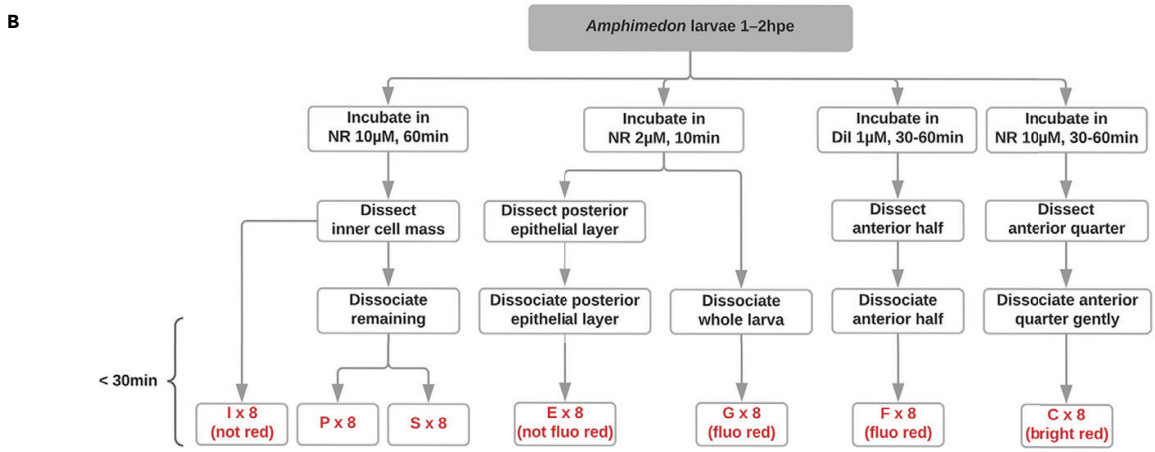

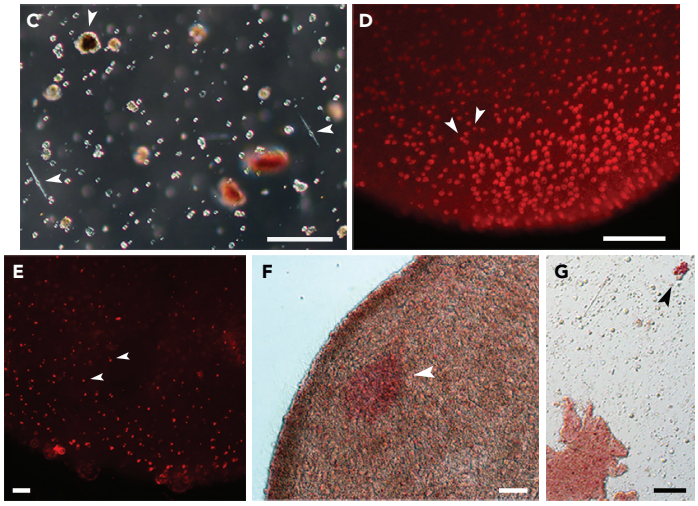

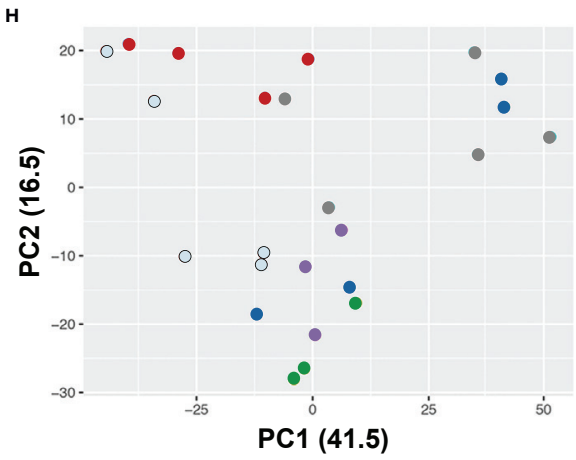

Figure 1. Identification and isolation of larval cell types and populations

(A) Diagram of the *Amphimedon queenslandica* larval body plan with cell types analyzed in this study highlighted (left) and a description of features used to identify dissociated cell types (right).

(B) Schematic of workflow for identifying and isolating larval cell types and pools. Red letters in flowchart correspond to cell types listed in the table in (A). (C–G) Arrowheads in plates (C–G) correspond to cell types indicated in Table (A). (C) Cluster of mixed dissociated cell types from larvae incubated in 10 μM neutral red (NR) for 60 min. Epithelial cells are red whereas cells of the inner cell mass (ICM) are off-white; sclerocytes and pigment ring cells (arrowheads) are identifiable by their elongated shape and dark brown pigment, respectively. (D) Anterior end of larva incubated with 2 μM NR for 10 min showing fluorescent red globular cells. (E) Anterior end of larva incubated in 1 μM CM-DiI for 30 min showing fluorescent red flask cells. (F and G) Anterior end of larva incubated in 10 μM NR for 30 min showing bright-red cuboidal cells, in contrast to surrounding auburn-red epithelial cells (F). This color contrast was retained in dissociated cells (G).

(H) Principle component analysis of the 500 most variably expressed genes in the CEL-Seq2 analysis of cell type and pool transcriptomes. Gene expression levels cluster approximately by larval cell type, with some overlap seen between globular cells and the ICM. PC1 and PC2 consist 58% of overall variation. hpe, hours post emergence; NR, Neutral Red dye; CM-DiI, Cell-Tracker™ CM-DiI dye. Scale bar: (C–E, G) 50 μm, (F) 100 μm. Larva illustration modified from (Richards, 2010), cell types not drawn to scale.

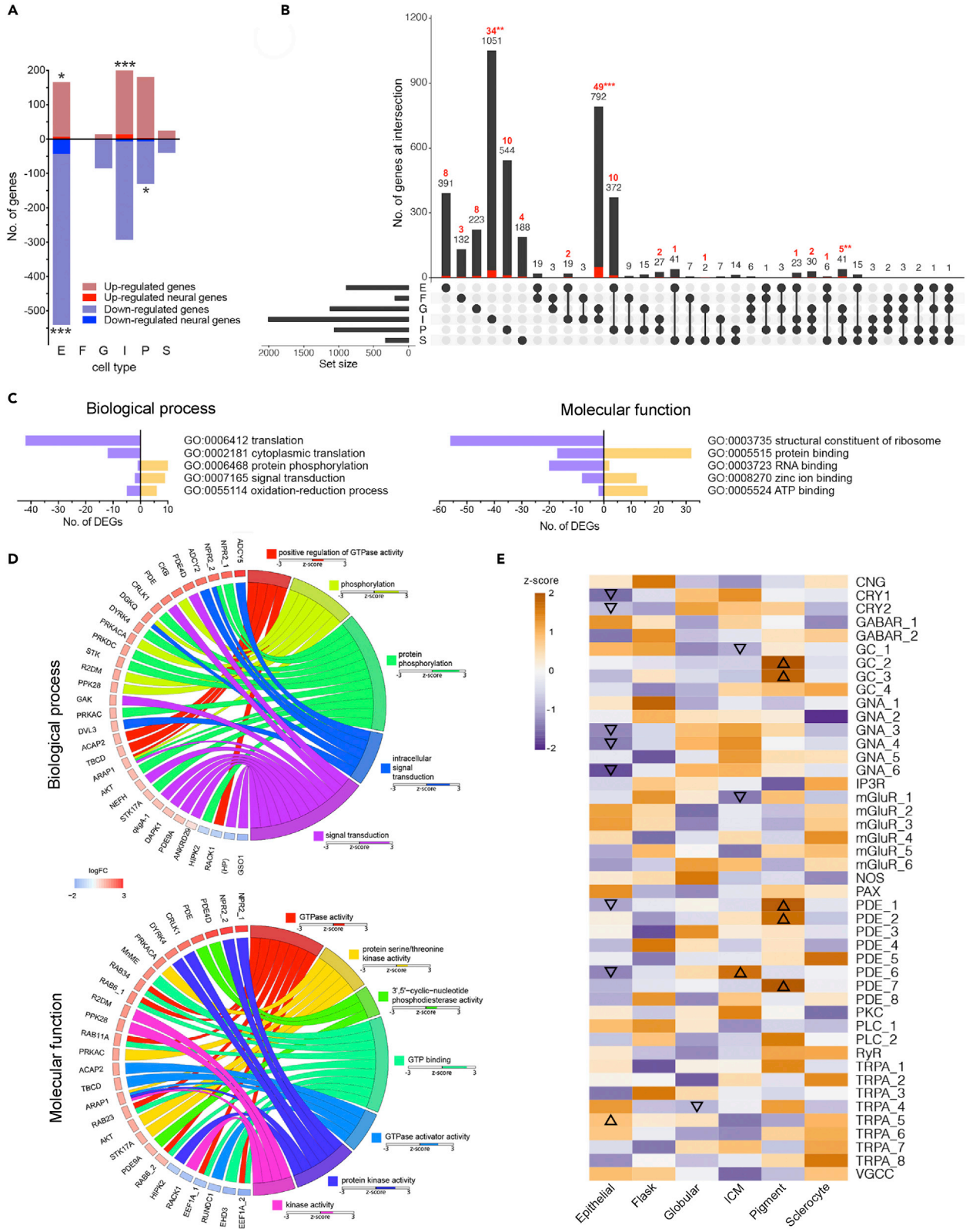
A
No. of genes
cell type
E F G I P S
Up-regulated genes
Up-regulated neural genes
Down-regulated genes
Down-regulated neural genes
B
No. of genes at intersection
Set size
C
Biological process
GO:0006412 translation
GO:0002181 cytoplasmic translation
GO:0006468 protein phosphorylation
GO:0007165 signal transduction
GO:0055114 oxidation-reduction process
No. of DEGs
Molecular function
GO:0003735 structural constituent of ribosome
GO:0005515 protein binding
GO:0003723 RNA binding
GO:0008270 zinc ion binding
GO:0005524 ATP binding
No. of DEGs
D
Biological process
positive regulation of GTPase activity
phosphorylation
protein phosphorylation
intracellular signal transduction
signal transduction
logFC
Molecular function
GTPase activity
protein serine/threonine kinase activity
3',5'-cyclic-nucleotide phosphodiesterase activity
GTP binding
GTPase activator activity
protein kinase activity
kinase activity
E
z-score
CNG
CRY1
CRY2
GABAR_1
GABAR_2
GC_1
GC_2
GC_3
GC_4
GNA_1
GNA_2
GNA_3
GNA_4
GNA_5
GNA_6
IP3R
mGluR_1
mGluR_2
mGluR_3
mGluR_4
mGluR_5
mGluR_6
NOS
PAX
PDE_1
PDE_2
PDE_3
PDE_4
PDE_5
PDE_6
PDE_7
PDE_8
PKC
PLC_1
PLC_2
RyR
TRPA_1
TRPA_2
TRPA_3
TRPA_4
TRPA_5
TRPA_6
TRPA_7
TRPA_8
VGCC
Epithelial
Flask
Globular
ICM
Pigment
Sclerocyte

Figure 2. Analysis of gene expression in posterior pigment ring cells and other larval cells

(A) Total number of genes significantly differentially expressed in given cell type/pool compared to all other larval cell types/pools combined. Neural genes are significantly upregulated in epithelial cells ($p = 0.043$) and in cells of the inner cell mass ($p < 0.001$), and downregulated in epithelial cells ($p < 0.001$) and pigment ring cells ($p = 0.014$).

(B) Number of genes significantly differentially expressed in pairwise comparisons. Columns show total numbers of genes uniquely upregulated (red, neural genes; black, all genes) in each cell type/pool (first six columns) and between cell types (the remaining columns). For instance, globular cells and inner cell mass were the most alike transcriptionally, having the most shared upregulated genes (792). Asterisks indicate significant enrichment of neural genes (genes upregulated in inner mass cells only: $p = 0.004$; in globular cells and inner mass cells: $p < 0.001$; in globular cells, inner mass cells and sclerocytes: $p = 0.002$). E, epithelial cell; F, flask cell; G, globular cell; I, inner cell mass; P, pigment ring cell; S, sclerocyte. *, $p < 0.05$; **, $p < 0.01$; ***, $p < 0.001$.

(C) Top five most enriched GO terms for genes significantly up- (orange bars) and downregulated (purple bars) in posterior pigment ring cells (see Figure S1 for GO enrichments in other larval cell types/pools).

(D) Chord diagrams displaying the relationship between differentially expressed genes and signaling-associated GO terms enriched in posterior pigment ring cells. Positive logFC (red) indicates upregulation. Positive z-scores of GO terms reflect a higher number of upregulated genes.

(E) Expression of genes with potential roles in photoreception, including ciliary and rhabdomeric phototransduction systems. At least one paralog of these gene families is expressed in pigment ring cells. Triangles indicate significant upregulation (upward pointing triangles) and downregulation (downward pointing triangles).

sponge-specific expansions, including members of the γ-aminobutyric acid receptor (GABAR), metabotropic glutamate receptor (mGluR), and transient receptor potential cation channel subfamily A (TRPA) (Kadowaki, 2015; Krishnan et al., 2014). We find that, for several gene families, at least one paralog is expressed in pigment ring cells (Figure 2E); two of the four GC and three of the eight PDE genes are significantly upregulated in pigment ring cells compared to other larval cell types (Figure 2E). Nitric oxide synthase (NOS), CRY1, and CRY2 cell type expression profiles match closely with previous *in situ* hybridization patterns (Jindrich et al., 2017; Rivera et al., 2012; Ueda et al., 2016).

Amphimedon larval phototaxis is impacted by agonists and antagonists of opsin-mediated phototransduction

Given the expression of conserved phototransducers in the pigment ring cells, we sought to determine if known agonists and antagonists of components of opsin-mediated phototransduction pathways (Table 1) affect *Amphimedon* larval phototaxis (Figure 3 and S3). Specifically, we recorded the movements of batches of 10 *Amphimedon* larvae subjected to diffuse unidirectional light in a 7.5 × 2.2 × 1.3 cm chamber (Figure 3A). The swimming behaviors of larvae, usually placed on the bright side of the chamber (Q1), were recorded and their position was scored at 5 sec intervals for 1 min. Specifically, at each time point, the larval position was assigned to a quartile along the light gradient. In control conditions (i.e. 0.22 μm-filtered seawater (FSW) and 1.5% DMSO in FSW), most larvae swim toward the darkest quartile of the chamber (Q4, here on referred to as "darkness") within 20 sec of being introduced into the brightest quartile (Q1, here on referred to as "brightness"); there is limited interquartile movement after 30 sec (Figure 3B, 3C, and Video S1).

PLC inhibitor

U-73122 is an inhibitor of PLC (Yule and Williams, 1992), which converts phosphatidylinositol 4,5-bisphosphate (PIP2) to diacylglycerol (DAG) and inositol 1,4,5-trisphosphate (IP3), and is involved in rhabdomeric photoreception (del Pilar Gomez and Nasi, 1998). Larvae pre-incubated in U-73122 do not respond negatively to light as normal; instead, most treated larvae remain in brightness (Q1) (Figure 3D and Video S2). U-73122-treated larvae not subjected to differential light also remain primarily in Q1 (Figure S3A) When U-73122-treated larvae commence from darkness (Q4), they swim toward brightness, indicating that they have become positively phototactic (Figure 3E).

Calcium signaling inhibitors

Calcium critically modulates photosignaling in both rhabdomeric and ciliary photoreceptors (Krizaj and Copenhagen, 2007; Tsuda, 1987); we therefore tested the effect of nifedipine, an L-type voltage-gated calcium channel (VGCC) inhibitor, on larval phototaxis. Larvae treated with nifedipine are less negatively phototactic than control larvae and behave similarly to larvae that are not exposed to unidirectional light (Figures 3B, 3C, 3F, and Video S3). This inhibitory effect reduces over longer pre-incubation times, with larvae pre-exposed to nifedipine for 30 min exhibiting normal phototactic behavior (Figure 3G and Table S3). This suggests that larvae are able to re-establish calcium homeostasis by an alternate pathway. Larvae treated with 2-aminoethoxydiphenyl borate (2-APB), an inhibitor of inositol trisphosphate receptor (IP3R), which releases calcium from the endoplasmic reticulum, exhibit normal phototaxis (Figure 3H).

Table 1. Reagents tested for effects on *Amphimedon* larval phototactic behavior

Reagent	Function	Solvent	Stock concentration	Working concentration	Pre-incubation time
L-glutamate	Neurotransmitter/mGluR agonist	FSW	20 mM	0.5 mM	30 min
AP3	mGluR antagonist	FSW	50 mM	0.5 mM	15 min
GABA	Neurotransmitter/GABAR agonist	FSW	280 mM	10 mM	30 min
Baclofen	GABAR agonist	FSW	15 mM	0.625 mM	30 min
2-OH-saclofen	GABAR antagonist	FSW	5 mM	0.1 mM	30 min
nifedipine	L-type VGCC antagonist	DMSO	10 mM	0.005 mM	none
U-73122	PLC inhibitor	DMSO	1 mM	0.3 μM	15 min
2-APB	IP3R antagonist	DMSO	10 mM	0.02 mM	15 min
staurosporine	PK inhibitor	DMSO	200 μM	0.01 μM	15 min
TPA	PKC agonist	DMSO	200 μM	0.1 μM	15 min
PTIO	NO scavenger	FSW	20 mM	0.25 mM	5 min
L-NAME	NOS inhibitor	FSW	100 mM	10 mM	15 min
cGMP	second messenger	FSW	10 mM	0.1 mM	15 min

2-APB, 2-aminoethyldipheylborate; 2-OH-saclofen, 2-hydroxy-saclofen; AP3, 2-amino-3-phosphonopropionic acid; cGMP, cyclic guanosine monophosphate; DMSO, dimethyl sulfoxide; GABA, gamma-aminobutyric acid; GABAR, gamma-aminobutyric acid receptor; IP3R, inositol triphosphate receptor; L-NAME, N_{ω}-Nitro-L-arginine methyl ester hydrochloride; mGluR, metabotropic glutamate receptor; NO, nitric oxide; NOS, nitric oxide synthase; PK, protein kinase; PLC, phospholipase C; PTIO, α-phenyl-4,4,5,5,-tetramethylimidazoline-1-oxyl-3-oxide; TPA, phorbol-12-myristate-13-acetate; VGCC, voltage-gated calcium channel.

Larvae exposed to 2-APB and nifedipine are negatively phototactic but show a delayed response (Figure S3).

Protein kinase modulators

Protein kinase C (PKC) mediates downstream phosphorylation events in phototransduction (del Pilar Gomez and Nasi, 1998). We found that staurosporine, a broad-spectrum protein kinase inhibitor, abolishes larval phototaxis, with larval movements akin to when unidirectional light is absent (Figures 3I, S3 and Table S3). In contrast, phorbol-12-myristate-13-acetate (TPA), a PKC agonist, does not alter phototaxis (Figure 3J). Although staurosporine is a broad-spectrum protein kinase inhibitor, the specificity of TPA is consistent with PKC being involved in larval phototaxis.

Second messenger and modulators

Nitric oxide (NO) is involved in sponge CRY-based photoreception (Müller et al., 2013) and metamorphosis (Song et al.,2021; Ueda et al., 2016). When treated with α-phenyltetramethylnitronyl nitroxide (PTIO), a NO scavenger, *Amphimedon* larvae are significantly more negatively phototactic than normal (Figure 3K). In contrast, cyclic guanosine monophosphate (cGMP), a second messenger produced by the PDE pathway of ciliary photoreceptors, does not alter phototaxis (Figure 3L).

mGluR & GABAR modulators

Glutamate (Glu) is a ligand for metabotropic glutamate receptors (mGluRs), a family of GPCRs related to opsins. Phototaxis is disrupted when larvae are pre-incubated with 0.5 mM Glu for a minimum of 30 min before being subjected to unidirectional light (Figures 3M, S3 and Table S3). Glu-treated larvae first swim toward darkness, but upon reaching the dark edge, promptly returned to brightness, unlike normal larvae (Video S4). This effect persists even when incubated larvae underwent the assay in FSW (Figure S3). Neither AP3 (mGluR antagonist) (Figure 3N) nor 2-OH-saclofen (GABAR antagonist) (Figure S3) affects phototaxis. Larvae treated with 10 mM GABA were significantly more negatively phototactic than untreated normal larvae (Figure S3 and Table S3).

Combinatorial impacts of agonists and antagonists

Having demonstrated that PLC, VGCC, PKC, and mGluR agonists and antagonists affect normal larval phototaxis, we used a combinatorial pharmacological approach to determine the relationship of these signaling pathway components to each other. We identified six combinations where inhibitors of normal

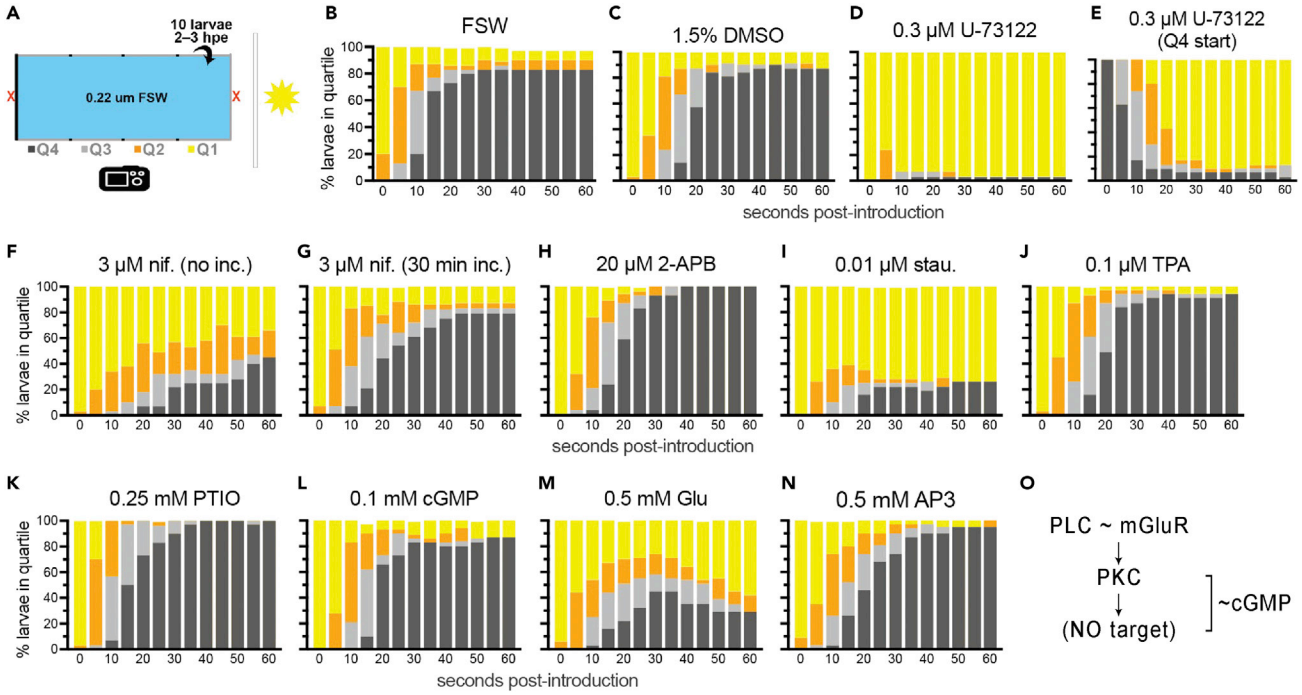

Figure 3. The effect of agonists and antagonists of bilaterian phototransduction pathways on *Amphimedon* larval phototaxis

(A) Assay chamber divided into four quartiles (Q1–Q4) for scoring purposes (see STAR Methods for details). Larvae were added directly into the bright end (Q1) with a pipette, their movements were filmed from above, and the number of larvae in each quartile (y-axis) at every 5 sec interval (x-axis) was scored over a total of one minute.

(B and C) Larval phototaxis in assay chambers under control treatments of FSW (B) and 1.5% DMSO in FSW (C). Larvae display normal negative phototaxis and differences between FSW and 1.5% DMSO are insignificant.

(D and E) Significant inhibition of negative phototaxis in larvae in the presence of 0.3 µM U-73122, a PLC inhibitor; larvae were pre-incubated in U-73122 for 15 min before being placed in the assay chamber (D). In contrast, 0.3 µM U-73122-treated larvae display abnormal positive phototaxis when introduced into the dark end (Q4) in this treatment (E).

(F and G) Significant inhibition of negative phototaxis with 3 µM nifedipine, a VGCC inhibitor with no pre-incubation (F). This inhibitory effect is reduced when larvae are pre-incubated for 30 min in 3 µM nifedipine (G).

(H) Treatment with the IP3R inhibitor, 20 µM 2-APB (15 min pre-incubation) does not affect normal negative phototaxis.

(I and J) Treatment with 0.01 µM staurosporine (15 min pre-incubation), a protein kinase inhibitor, blocks normal negative phototaxis (I), while 0.1 µM TPA (15 min pre-incubation), a PKC agonist, has no impact on phototaxis (J).

(K and L) Neither 0.25 mM PTIO (5 min pre-incubation), a NO scavenger (K), nor 0.1 mM cGMP (15 min pre-incubation), a second messenger (L), obliterates phototaxis.

(M) Larvae pre-incubated for 30 min in 0.5 mM Glu show a marked decrease in normal negative phototaxis.

(N) 0.5 mM AP3 (15 min pre-incubation), an mGluR antagonist, does not have a significant impact on larval phototaxis.

(O) Photoassays, when performed using combinations of two reagents of antagonistic effects, allow the reconstruction of the phototransduction pathway. "~" indicates unconfirmed cascade between two targets. Raw counts and details of all statistics are available from Table S3.

negative phototaxis can be changed by a second reagent. Specifically, (i) the PKC agonist TPA, the NO scavenger PTIO, and the second messenger cGMP each reverses the effect of the PLC inhibitor U-73122, (ii) TPA and cGMP also overcome the inhibitory effect of Glu, and (iii) PTIO overcomes the effect of the PKC inhibitor staurosporine (Table S3).

With the assumption that both staurosporine and TPA operate on the same target, it appears PLC and mGluR are both upstream of cGMP and PKC, the latter of which is upstream of a NO target (Figure 3O). The placement of VGCC in this pathway is uncertain, as none of the restorative agents rescue the inhibitory effect of nifedipine to a level that is statistically indifferent from controls.

DISCUSSION

Here, we build on previous studies that have implicated CRY and the NO-GC-cGMP pathway in the negative phototactic behavior of *Amphimedon queenslandica* larvae (Song et al 2021; Say and Degnan, 2019; Ueda et al., 2016) by providing two lines of evidence for the involvement of intracellular signaling mechanisms similar to those found in bilaterian opsin-based photosystems: (i) larval cell type transcriptomics, and (ii) the effect of agonists and antagonists of components of bilaterian phototransduction pathways on larval phototaxis. Our results suggest that sponge larval phototaxis uses similar intracellular signaling mechanisms to bilaterians. These similarities are striking because the sponge photosensory system is aneural and appears to only require the stereotypic ciliary behavior of individual posterior pigment ring cells to respond to directional light. No evidence had thus far suggested the involvement of intercellular interactions for phototaxis to function in this sponge.

Despite expressing a deficiency of neural genes compared to other larval cell types, posterior pigment ring cells are significantly enriched in signal transducers that comprise opsin-based phototransduction pathways. For instance, two of the four GC genes and three of the eight *Amphimedon* PDE genes are significantly upregulated, and one of the two PLC genes is highly expressed in the pigment ring. GC, PDE, and PLC are key signal transducers of ciliary and rhabdomeric opsin pathways, initiated through the binding of Goα, Gtα, and Gqα (Lamb, 2013; Leung and Montell, 2017; Oakley and Pankey, 2008; Plachetzki and Oakley, 2007). Although *Amphimedon* possess a Gtα gene and two Gqα genes (Krishnan and Schiöth, 2015; Lokits et al., 2018), they are not differentially expressed in the pigment ring over other cell types, providing no support for the use of one pathway over another. However, the larval behavioral assays suggest that the immediate downstream targets of the PLC pathway are conserved. Dramatically, treatment with U-73122, which inhibits PLC-mediated conversion of PIP_2 to IP_3 and DAG, changes larvae from being negatively to positively phototactic. Given that IP_3 normally induces the release of internally stored calcium (Dawson, 1997), the inhibition of PLC might be expected to have a similar effect to an IP3R inhibitor. Instead, PLC inhibition appears to cause the long posterior cilia (LPC) in the pigment ring to respond opposite to normal. Although the specific mechanisms of how this occurs are unknown, it appears that the IP_3 and/or DAG second messengers are necessary for the correct interpretation of directional light by LPC cells in the posterior pigment ring.

Both our transcriptomic and behavioral data support the GPCR pathway being engaged in photosignaling in *Amphimedon*. GPCRs also appear to regulate the initiation of *Amphimedon* metamorphosis by interacting with the photosensory system (Say and Degnan, 2019). We found that Glu produced a delayed (30 min) inhibitory effect on phototaxis (Figure S3), and given its upstream placement within the signaling cascade (Figure 3O), we suggest that a glutamate receptor may be playing a role akin to opsins in initiating a largely conserved GPCR cascade to endow photosensitivity. How the role of GPCRs integrates with that of CRY remains to be elucidated, although CRY may also regulate sponge photosignaling through its interaction with NOS (Müller et al., 2013). In addition, Glu-treated *Amphimedon* larvae, although showing no visible mobility impairment in the horizontal sense, appear to swim deeper than normal larvae (unpublished data). This suggests an additional role of GPCR pathways in cilia-mediated locomotion, as is present in protists to neural metazoans (Bucci et al., 2005; Devlin and Schlosser, 1999; Elliott and Leys, 2010; Parnas et al., 1999; Perovic et al., 1999; Romanova et al., 1996), and in invertebrate swimming larvae (Katow et al., 2013). Together, these observations suggest that the animal visual-motor circuit evolved from an ancient signaling system that predates metazoan multicellularity.

A role for calcium signaling in *Amphimedon* larval phototaxis is supported by the upregulation of CRLK and the strong photoinhibitory effect of the VGCC-inhibitor nifedipine. The weak (statistically insignificant) effect of 2-APB, an IP3R inhibitor, on larval phototaxis (Figure 3H) suggests that an influx of extracellular calcium may have a greater influence than stored calcium release on this photosensory response. Furthermore, nifedipine's incomplete inhibition of intracellular calcium increase following light exposure (Figure 3F) suggests potential involvement of other cation channels. Given the ubiquity and pleiotropy of calcium signaling (Clapham, 2007), we suggest that the immediate inhibitory effect of nifedipine on phototaxis implies that VGCC-modulated calcium flux may be more tightly associated with the directional movement in the LPC in the pigment ring; the LPC acts to steer *Amphimedon* larvae toward darkness (Leys and Degnan, 2001). Similar cross-membrane calcium fluxes modulate cilia movement in protists (Lodh et al., 2016; Murakami and Eckert, 1972; Pala et al., 2017).

Our findings lend support to the proposition that components of the opsin-based photosystems that are present in neural animals contribute to *Amphimedon* photosensory functioning. These include key transducers of opsin-based photosystem subtypes that have diverged in neural animals, including PLC (Gqα-mediated transduction known in flies), PDE (Gtα-mediated transduction known in vertebrates), and GC (Goα-mediated transduction known in molluscs). Their expression in sponge larval pigment ring cells and their apparent function in phototaxis in this animal, both are consistent with an ancestral photosystem comprising these signaling components operating in the last common ancestor of metazoans. These observations, combined with the known co-functioning of ciliary and rhabdomeric photosystems in some animals (Arendt, 2004; Verasztó et al., 2018), suggest that these photosystems, which are distinct in many extant animals, may have been originally integrated. However, because the base of the metazoan tree is currently unresolved (Feuda et al., 2017; Halanych et al., 2016; Moroz et al., 2014; Redmond and McLysaght, 2021; Whelan et al., 2015), it is unclear whether this is the ancestral state, or a derived condition. Regardless of the phyletic branching order at the base of the metazoan tree, this study suggests the first metazoan photosensory systems used a deeply conserved set of signal transducers that function in extant neural and aneural animal photosystems. The enrichment of expressed genes encoding conserved neurogenic transcription factors in the larval pigment ring lends support to this proposition (Adamska et al., 2007; Richards et al., 2008; Richards and Degnan, 2012).

Limitations of the study

By using cell-specific transcriptomic analyses and pharmacological manipulations on different components of intracellular signal transduction pathways, this study provides evidence that the aneural sponge *Amphimedon queenslandica* share an ancestral set of signaling molecules used by neural metazoans for light-induced phototaxis behavior. Although our data suggest important roles for GPCR- and calcium-mediated signal transduction pathways in light-induced phototaxis behavior, we cannot unequivocally conclude that these pathways are involved in the *Amphimedon* phototransduction pathway. Direct intracellular recordings and calcium imaging experiments in pigment cells (and other cell types) upon light stimulation would provide a supporting line of evidence for the presence of GPCR- and calcium-mediated photoreception in sponges.

STAR★METHODS

Detailed methods are provided in the online version of this paper and include the following:

- KEY RESOURCES TABLE
- RESOURCE AVAILABILITY
  - Lead contact
  - Materials availability
  - Data and code availability
- EXPERIMENTAL MODEL AND SUBJECT DETAILS
  - Animals
- METHOD DETAILS
  - Isolation of larval cell types for CEL-Seq2
  - CEL-Seq2
  - CEL-Seq2 analysis pipeline
  - Gene function analysis
  - Domain analysis
  - Phototaxis assays
- QUANTIFICATION AND STATISTICAL ANALYSIS
  - Differential gene expression analysis
  - Phototaxis assay analysis

SUPPLEMENTAL INFORMATION

Supplemental information can be found online at https://doi.org/10.1016/j.isci.2022.104436.

ACKNOWLEDGMENTS

This research was supported by Australian Research Council (ARC) awards to BMD and SMD. VA was supported by funding from the Clem Jones Centre for Ageing Dementia Research. We thank Joanne Leerberg, Kerry Roper, Gemma Richards, Xueyan Xiang, HaoJing Shao, Brooke Gardiner, and Janette Edson for their comments on the manuscript and their generous assistance on various stages of the experiments and on

sequencing. We are grateful to Nick Rhodes (QCIF) for computational support. Heron Island Research Station provided a research scholarship to EW that fostered field components of this study.

AUTHOR CONTRIBUTIONS

EW, SMD, and BMD conceived the study. All authors were engaged in experiment design. EW performed all experiments and analyzed data with critical input from VA, SRW, SMD, and BMD. EW and BMD drafted the manuscript with comments from SMD, VA, and SRW. All authors read and edited the final manuscript.

DECLARATION OF INTERESTS

The authors declare no competing interests.

Received: February 1, 2021
Revised: August 22, 2021
Accepted: May 17, 2022
Published: June 17, 2022

REFERENCES

Adamska, M., Degnan, S.M., Green, K.M., Adamski, M., Craigie, A., Larroux, C., and Degnan, B.M. (2007). Wnt and TGF-β expression in the sponge *Amphimedon queenslandica* and the origin of metazoan embryonic patterning. PLoS One *2*, e1031. https://doi.org/10.1371/journal.pone.0001031.

Arendt, D., Tessmar-Raible, K., Snyman, H., Dorresteijn, A.W., and Wittbrodt, J. (2004). Ciliary photoreceptors with a vertebrate-type opsin in an invertebrate brain. Science *306*, 869–871. https://doi.org/10.1126/science.1099955.

Arendt, D., and Wittbrodt, J. (2001). Reconstructing the eyes of urbilateria. Philos. Trans. R. Soc. B Biol. Sci. *356*, 1545–1563. https://doi.org/10.1098/rstb.2001.0971.

Arendt, D., Hausen, H., and Purschke, G. (2009). The "division of labour" model of eye evolution. Philos. Trans. R. Soc. B Biol. Sci. *364*, 2809–2817. https://doi.org/10.1098/rstb.2009.0104.

Bates, D., Mächler, M., Bolker, B., and Walker, S. (2015). Fitting linear mixed-effects models using lme4. J. Stat. Softw. *67*, 1–48. https://doi.org/10.18637/jss.v067.i01.

Bettler, B., Kaupmann, K., Mosbacher, J., Gassmann, M., Kaupmann, K., Mosbacher, J., Gassmann, M., and Structure, M. (2004). Molecular structure and physiological functions of GABAB receptors. Physiol. Rev. *84*, 835–867. https://doi.org/10.1152/physrev.00036.2003.

Bucci, G., Ramoino, P., Diaspro, A., and Usai, C. (2005). A role for GABAA receptors in the modulation of *Paramecium* swimming behavior. Neurosci. Lett. *386*, 179–183. https://doi.org/10.1016/j.neulet.2005.06.006.

Cashmore, A.R., Jarillo, J.A., Wu, Y.J., and Liu, D. (1999). Cryptochromes: blue light receptors for plants and animals. Science *284*, 760–765. https://doi.org/10.1126/science.284.5415.760.

Chen, S., Zhou, Y., Chen, Y., and Gu, J. (2018). Fastp: an ultra-fast all-in-one FASTQ preprocessor. Bioinformatics *34*, i884–i890. https://doi.org/10.1093/bioinformatics/bty560.

Chrachri, A., Nelson, L., and Williamson, R. (2005). Whole-cell recording of light-evoked photoreceptor responses in a slice preparation of the cuttlefish retina. Vis. Neurosci. *22*, 359–370. https://doi.org/10.1017/s0952523805223106.

Clapham, D.E. (2007). Calcium signaling. Cell *131*, 1047–1058. https://doi.org/10.1016/j.cell.2007.11.028.

Conesa, A., Götz, S., Garcia-Gomez, J.M., Terol, J., Talón, M., and Robles, M. (2005). Blast2GO: a universal tool for annotation, visualization and analysis in functional genomics research. Bioinformatics *21*, 3674–3676. https://doi.org/10.1093/bioinformatics/bti610.

Conn, P., Strong, J., and Kaczmarek, L. (1989). Inhibitors of protein kinase C prevent enhancement of calcium current and action potentials in peptidergic neurons of *Aplysia*. J. Neurosci. *9*, 480–487. https://doi.org/10.1523/jneurosci.09-02-00480.1989.

Conway, J.R., Lex, A., and Gehlenborg, N. (2017). UpSetR: an R package for the visualization of intersecting sets and their properties. Bioinformatics *33*, 2938–2940. https://doi.org/10.1093/bioinformatics/btx364.

Dawson, A.P. (1997). Calcium signalling: how do IP3 receptors work? Curr. Biol. *7*, R544–R547. https://doi.org/10.1016/s0960-9822(06)00277-6.

Gomez, M.d.P., and Nasi, E. (1998). Membrane current induced by protein kinase C activators in rhabdomeric photoreceptors: implications for visual excitation. J. Neurosci. *18*, 5253–5263. https://doi.org/10.1523/jneurosci.18-14-05253.1998.

Gomez, M.d.P., and Nasi, E. (2000). Light transduction in invertebrate hyperpolarizing photoreceptors: possible involvement of a Go-regulated guanylate cyclase. J. Neurosci. *20*, 5254–5263. https://doi.org/10.1523/jneurosci.20-14-05254.2000.

DeRiemer, S.A., Strong, J., Albert, K., Greengard, P., and Kaczmarek, L. (1985). Enhancement of calcium current in *Aplysia* neurones by phorbol ester and protein kinase C. Nature *313*, 313–316. https://doi.org/10.1038/313313a0.

Devlin, C.L., and Schlosser, W. (1999). γ-Aminobutyric acid modulation of acetylcholine-induced contractions of a smooth muscle from an echinoderm (*Sclerodactyla briareus*). Invert Neurosci. *4*, 1–8. https://doi.org/10.1007/s101580050001.

Dorlöchter, M., and Stieve, H. (1997). The *Limulus* ventral photoreceptor: light response and the role of calcium in a classic preparation. Prog. Neurobiol. *53*, 451–515. https://doi.org/10.1016/s0301-0082(97)00046-4.

Ebanks, S.C., O'Donnell, M.J., and Grosell, M. (2010). Characterization of mechanisms for Ca2+ and HCO3–/CO32– acquisition for shell formation in embryos of the freshwater common pond snail *Lymnaea stagnalis*. J. Exp. Biol. *213*, 4092–4098. https://doi.org/10.1242/jeb.045088.

Elliott, G.R.D., and Leys, S.P. (2010). Evidence for glutamate, GABA and NO in coordinating behaviour in the sponge, *Ephydatia muelleri* (Demospongiae, Spongillidae). J. Exp. Biol. *213*, 2310–2321. https://doi.org/10.1242/jeb.039859.

Elliott, G.R.D., Macdonald, T.A., and Leys, S.P. (2004). Sponge larval phototaxis: a comparative study. Boll. Mus. Ist. Biol. Univ. Genova *68*, 291–300.

Ellwanger, K., and Nickel, M. (2006). Neuroactive substances specifically modulate rhythmic body contractions in the nerveless metazoon *Tethya wilhelma* (Demospongiae, Porifera). Front. Zool. *3*, 7. https://doi.org/10.1186/1742-9994-3-7.

Ellwanger, K., Eich, A., and Nickel, M. (2007). GABA and glutamate specifically induce contractions in the sponge *Tethya wilhelma*. J. Comp. Physiol. A. *193*, 1–11. https://doi.org/10.1007/s00359-006-0165-y.

Fain, G.L., Hardie, R., and Laughlin, S.B. (2010). Phototransduction and the evolution of photoreceptors. Curr. Biol. *20*, R114–R124. https://doi.org/10.1016/j.cub.2009.12.006.

Fein, A., and Cavar, S. (2000). Divergent mechanisms for phototransduction of invertebrate microvillar photoreceptors. Vis.

Neurosci. *17*, 911–917. https://doi.org/10.1017/s0952523800176102.

Fernandez-Valverde, S.L., Calcino, A.D., and Degnan, B.M. (2015). Deep developmental transcriptome sequencing uncovers numerous new genes and enhances gene annotation in the sponge *Amphimedon queenslandica*. BMC Genomics *16*, 387–397. https://doi.org/10.1186/s12864-015-1588-z.

Feuda, R., Dohrmann, M., Pett, W., Philippe, H., Rota-Stabelli, O., Lartillot, N., Wörheide, G., and Pisani, D. (2017). Improved modeling of compositional heterogeneity supports sponges as sister to all other animals. Curr. Biol. *27*, 3864–3870.e4. https://doi.org/10.1016/j.cub.2017.11.008.

Feuda, R., Hamilton, S.C., McInerney, J.O., and Pisani, D. (2012). Metazoan opsin evolution reveals a simple route to animal vision. Proc. Natl. Acad. Sci. U S A *109*, 18868–18872. https://doi.org/10.1073/pnas.1204609109.

Feuda, R., Rota-Stabelli, O., Oakley, T.H., and Pisani, D. (2014). The comb jelly opsins and the origins of animal phototransduction. Genome Biol. Evol. *6*, 1964–1971. https://doi.org/10.1093/gbe/evu154.

Finn, R.D., Coggill, P., Eberhardt, R.Y., Eddy, S.R., Mistry, J., Mitchell, A.L., Potter, S.C., Punta, M., Qureshi, M., Sangrador-Vegas, A., et al. (2016). The Pfam protein families database: towards a more sustainable future. Nucleic Acids Res. *44*, D279–D285. https://doi.org/10.1093/nar/gkv1344.

Fulton, D., Condro, M.C., Pearce, K., and Glanzman, D.L. (2008). The potential role of postsynaptic phospholipase C activity in synaptic facilitation and behavioral sensitization in *Aplysia*. J. Neurophysiol. *100*, 108–116. https://doi.org/10.1152/jn.90389.2008.

Galione, A., White, A., Willmott, N., Turner, M., Potter, B.V.L., and Watson, S.P. (1993). cGMP mobilizes intracellular Ca2+ in sea urchin eggs by stimulating cyclic ADP-ribose synthesis. Nat. Lett. *365*, 456–459. https://doi.org/10.1038/365456a0.

Gehring, W.J. (2014). The evolution of vision. Wiley Interdiscip. Rev. Dev. Biol. *3*, 1–40. https://doi.org/10.1002/wdev.96.

Grün, D., and Van Oudenaarden, A. (2015). Design and analysis of single-cell sequencing experiments. Cell *163*, 799–810. https://doi.org/10.1016/j.cell.2015.10.039.

Halanych, K.M., Whelan, N.V., Kocot, K.M., Kohn, A.B., and Moroz, L.L. (2016). Miscues misplace sponges. Proc. Natl. Acad. Sci. U S A *113*. 201525332. https://doi.org/10.1073/pnas.1525332113.

Hashimshony, T., Senderovich, N., Avital, G., Klochendler, A., de Leeuw, Y., Anavy, L., Gennert, D., Li, S., Livak, K.J., Rozenblatt-rosen, O., et al. (2016). CEL-Seq2: sensitive highly-multiplexed single-cell RNA-Seq. Genome Biol. *17*, 77. https://doi.org/10.1186/s13059-016-0938-8.

Jékély, G. (2009). Evolution of phototaxis. Philos. Trans. R. Soc. B Biol. Sci. *364*, 2795–2808. https://doi.org/10.1098/rstb.2009.0072.

Jindrich, K., Roper, K.E., Lemon, S., Degnan, B.M., Reitzel, A.M., and Degnan, S.M. (2017). Origin of the animal circadian clock: diurnal and light-entrained gene expression in the sponge *Amphimedon queenslandica*. Front. Mar. Sci. *4*, 327. https://doi.org/10.3389/fmars.2017.00327.

Jones, P., Binns, D., Chang, H.-Y., Fraser, M., Li, W., McAnulla, C., McWilliam, H., Maslen, J., Mitchell, A., Nuka, G., et al. (2014). InterProScan 5: genome-scale protein function classification. Bioinformatics *30*, 1236–1240. https://doi.org/10.1093/bioinformatics/btu031.

Kadowaki, T. (2015). Evolutionary dynamics of metazoan TRP channels. Pflugers Arch. Eur. J. Physiol. *467*, 2043–2053. https://doi.org/10.1007/s00424-015-1705-5.

Katow, H., Abe, K., Katow, T., Zamani, A., and Abe, H. (2013). Development of the GABA-ergic signaling system and its role in larval swimming in sea urchin. J. Exp. Biol. *216*, 1704–1716. https://doi.org/10.1242/jeb.074856.

Koyanagi, M., Takano, K., Tsukamoto, H., Ohtsu, K., Tokunaga, F., and Terakita, A. (2008). Jellyfish vision starts with cAMP signaling mediated by opsin-Gs cascade. Proc. Natl. Acad. Sci. U S A *105*, 15576–15580. https://doi.org/10.1073/pnas.0806215105.

Krishnan, A., and Schiöth, H.B. (2015). The role of G protein-coupled receptors in the early evolution of neurotransmission and the nervous system. J. Exp. Biol. *218*, 562–571. https://doi.org/10.1242/jeb.110312.

Krishnan, A., Dnyansagar, R., Almén, M.S., Williams, M.J., Fredriksson, R., Manoj, N., and Schiöth, H.B. (2014). The GPCR repertoire in the demosponge *Amphimedon queenslandica*: insights into the GPCR system at the early divergence of animals. BMC Evol. Biol. *14*, 270–283. https://doi.org/10.1186/s12862-014-0270-4.

Krizaj, D., and Copenhagen, D.R. (2002). Calcium regulation in photoreceptors. Front. Biosci. *7*, d2023–d2044.

Lamb, T.D. (2013). Evolution of phototransduction, vertebrate photoreceptors and retina. Prog. Retin. Eye Res. *36*, 52–119. https://doi.org/10.1016/j.preteyeres.2013.06.001.

Leung, N.Y., and Montell, C. (2017). Unconventional roles of opsins. Annu. Rev. Cell Dev. Biol. *33*, 241–264. https://doi.org/10.1146/annurev-cellbio-100616-060432.

Leys, S.P., and Degnan, B.M. (2001). Cytological basis of photoresponsive behavior in a sponge larva. Biol. Bull. *201*, 323–338. https://doi.org/10.2307/1543611.

Leys, S.P., Cronin, T.W., Degnan, B.M., and Marshall, J.N. (2002). Spectral sensitivity in a sponge larva. J. Comp. Physiol. A. Neuroethol. Sensory, Neural Behav. Physiol. *188*, 199–202. https://doi.org/10.1007/s00359-002-0293-y.

Lodh, S., Yano, J., Valentine, M.S., and Van Houten, J.L. (2016). Voltage-gated calcium channels of *Paramecium* cilia. J. Exp. Biol. *219*, 3028–3038. https://doi.org/10.1242/jeb.141234.

Lokits, A.D., Indrischek, H., Meiler, J., Hamm, H.E., and Stadler, P.F. (2018). Tracing the evolution of the heterotrimeric G protein α subunit in Metazoa. BMC Evol. Biol. *18*, 51. https://doi.org/10.1186/s12862-018-1147-8.

Love, M.I., Huber, W., and Anders, S. (2014). Moderated estimation of fold change and dispersion for RNA-seq data with DESeq2. Genome Biol. *15*, 550. https://doi.org/10.1186/s13059-014-0550-8.

Luo, D.G., Su, C.Y., and Yau, K.W. (2009). Photoreceptors: physiology. Encycl. Neurosci. 677–686. https://doi.org/10.1016/b978-008045046-9.00913-x.

Maldonado, M., Durfort, M., McCarthy, D.A., and Young, C.M. (2003). The cellular basis of photobehavior in the tufted parenchymella larva of demosponges. Mar. Biol. *143*, 427–441. https://doi.org/10.1007/s00227-003-1100-1.

Matzel, L.D., Muzzio, I.A., and Rogers, R.F. (1995). Diverse current and voltage responses to baclofen in an identified molluscan photoreceptor. J. Neurophysiol. *74*, 506–518. https://doi.org/10.1152/jn.1995.74.2.506.

Michael, A.K., Fribourgh, J.L., Van Gelder, R.N., and Partch, C.L. (2017). Animal cryptochromes: divergent roles in light perception, circadian timekeeping and beyond. Photochem. Photobiol. *93*, 128–140. https://doi.org/10.1111/php.12677.

Montell, C. (2012). *Drosophila* visual transduction. Trends Neurosci. *35*, 356–363. https://doi.org/10.1016/j.tins.2012.03.004.

Moran, Y., Barzilai, M.G., Liebeskind, B.J., and Zakon, H.H. (2015). Evolution of voltage-gated ion channels at the emergence of Metazoa. J. Exp. Biol. *218*, 515–525. https://doi.org/10.1242/jeb.110270.

Moroz, L.L., Kocot, K.M., Citarella, M.R., Dosung, S., Norekian, T.P., Povolotskaya, I.S., Grigorenko, A.P., Dailey, C., Berezikov, E., Buckley, K.M., et al. (2014). The ctenophore genome and the evolutionary origins of neural systems. Nature *510*, 109–114. https://doi.org/10.1038/nature13400.

Müller, W.E.G., Schröder, H.C., Markl, J.S., Grebenjuk, V.A., Korzhev, M., Steffen, R., and Wang, X. (2013). Cryptochrome in sponges: a key molecule linking photoreception with phototransduction. J. Histochem. Cytochem. *61*, 814–832. https://doi.org/10.1369/0022155413502652.

Murakami, A., and Eckert, R. (1972). Cilia: activation coupled to mechanical stimulation by calcium influx. J. Clin. Endocrinol. Metab. *175*, 1375–1377. https://doi.org/10.1126/science.175.4028.1375.

Nagy, K., and Contzen, K. (1997). Inhibition of phospholipase C by U-73122 blocks one component of the receptor current in *Limulus* photoreceptor. Vis. Neurosci. *14*, 995–998. https://doi.org/10.1017/s0952523800011706.

Nakanishi, N., Sogabe, S., and Degnan, B.M. (2014). Evolutionary origin of gastrulation: insights from sponge development. BMC Biol.

12, 26–29. https://doi.org/10.1186/1741-7007-12-26.

Nakanishi, N., Stoupin, D., Degnan, S.M., and Degnan, B.M. (2015). Sensory flask cells in sponge larvae regulate metamorphosis via calcium signaling. Integr. Comp. Biol. *55*, 1018–1027. https://doi.org/10.1093/icb/icv014.

Oakley, T.H., and Pankey, M.S. (2008). Opening the "black box": the genetic and biochemical basis of eye evolution. Evol. Educ. Outreach *1*, 390–402. https://doi.org/10.1007/s12052-008-0090-3.

Oakley, T.H., and Speiser, D.I. (2015). How complexity originates: the evolution of animal eyes. Annu. Rev. Ecol. Evol. Syst. *46*, 237–260. https://doi.org/10.1146/annurev-ecolsys-110512-135907.

Okazaki, Y., and Shizuri, Y. (2000). Effect of inducers and inhibitors on the expression of *bcs* genes involved in cypris larval attachment and metamorphosis of the barnacles *Balanus amphitrite*. Int. J. Dev. Biol. *44*, 451–456.

Pala, R., Alomari, N., and Nauli, S.M. (2017). Primary cilium-dependent signaling mechanisms. Int. J. Mol. Sci. *18*, 2272. https://doi.org/10.3390/ijms18112272.

Parnas, I., Rashkovan, G., Ong, J., and Kerr, D.I.B. (1999). Tonic activation of presynaptic GABAB receptors in the opener neuromuscular junction of crayfish. J. Neurophysiol. *81*, 1184–1191. https://doi.org/10.1152/jn.1999.81.3.1184.

Perovic, S., Krasko, A., Prokic, I., Muller, I.M., Muller, W.E.G., Müller, I.M., and Müller, W.E.G. (1999). Origin of neuronal-like receptors in Metazoa: cloning of a metabotropic glutamate/GABA-like receptor from the marine sponge Geodia cydonium. Cell Tissue Res *296*, 395–404. https://doi.org/10.1007/s004410051299.

Plachetzki, D.C., and Oakley, T.H. (2007). Key transitions during the evolution of animal phototransduction: novelty, "tree-thinking" co-option, and co-duplication. Integr. Comp. Biol. *47*, 759–769. https://doi.org/10.1093/icb/icm050.

Plachetzki, D.C., Fong, C.R., and Oakley, T.H. (2010). The evolution of phototransduction from an ancestral cyclic nucleotide gated pathway. Proc. R. Soc. B Biol. Sci. *277*, 1963–1969. https://doi.org/10.1098/rspb.2009.1797.

Ramirez, M.D., Pairett, A.N., Pankey, M.S., Serb, J.M., Speiser, D.I., Swafford, A.J., and Oakley, T.H. (2016). The last common ancestor of most bilaterian animals possessed at least nine opsins. Genome Biol. Evol. *8*, 3640–3652. https://doi.org/10.1093/gbe/evw248.

Ranganathan, R., Harris, W.A., and Zuker, C.S. (1991). The molecular genetics of invertebrate phototransduction. Trends Neurosci. *14*, 486–493. https://doi.org/10.1016/0166-2236(91)90060-8.

Rayer, B., Naynert, M., and Stieve, H. (1990). Phototransduction: different mechanisms in vertebrates and invertebrates. J. Photochem. Photobiol. *7*, 107–148. https://doi.org/10.1016/1011-1344(90)85151-l.

Redmond, A.K., and McLysaght, A. (2021). Evidence for sponges as sister to all other animals from partitioned phylogenomics with mixture models and recoding. Nat. Commun. *12*, 1783. https://doi.org/10.1038/s41467-021-22074-7.

Renard, E., Vacelet, J., Gazave, E., Lapébie, P., Borchiellini, C., and Ereskovsky, A.V. (2009). Origin of the neuro-sensory system: new and expected insights from sponges. Integr. Zool. *4*, 294–308. https://doi.org/10.1111/j.1749-4877.2009.00167.x.

Richards, G.S. (2010). The Origins of Cell Communication in the Animal Kingdom: Notch Signalling during Embryogenesis and Metamorphosis of the Demosponge Amphimedon Queenslandica. (Doctoral dissertation) (University of Queensland).

Richards, G.S., and Degnan, B.M. (2012). The expression of Delta ligands in the sponge *Amphimedon queenslandica* suggests an ancient role for Notch signaling in metazoan development. Evodevo *3*, 15. https://doi.org/10.1186/2041-9139-3-15.

Richards, G.S., Simionato, E., Perron, M., Adamska, M., Vervoort, M., Degnan, B.M., Vervoort, M., Perron, M., Richards, G.S., Simionato, E., et al. (2008). Sponge genes provide new insight into the evolutionary origin of the neurogenic circuit. Curr. Biol. *18*, 1156–1161. https://doi.org/10.1016/j.cub.2008.06.074.

Rivera, A.S., Ozturk, N., Fahey, B., Plachetzki, D.C., Degnan, B.M., Sancar, A., and Oakley, T.H. (2012). Blue-light-receptive cryptochrome is expressed in a sponge eye lacking neurons and opsin. J. Exp. Biol. *215*, 1278–1286. https://doi.org/10.1242/jeb.067140.

Romanova, E.V., Rubakhin, S.S., and S-Rózsa, K. (1996). Behavioral changes induced by GABA-receptor agonists in Lymnaea stagnalis L. Gen. Pharmacol. *27*, 1067–1071. https://doi.org/10.1016/0306-3623(95)00122-0.

Say, T.E., and Degnan, S.M. (2019). Molecular and behavioural evidence that interdependent photo - and chemosensory systems regulate larval settlement in a marine sponge. Mol. Ecol. *29*, 247–261. https://doi.org/10.1111/mec.15318.

Senatore, A., Raiss, H., and Le, P. (2016). Physiology and evolution of voltage-gated calcium channels in early diverging animal phyla: Cnidaria, Placozoa, Porifera and Ctenophora. Front. Physiol. *7*, 481. https://doi.org/10.3389/fphys.2016.00481.

Sha, Y., Phan, J.H., and Wang, M.D. (2015). Effect of low-expression gene filtering on detection of differentially expressed genes in RNA-seq data. Conf. Proc. IEEE Eng. Med. Biol. Soc. 6461–6464. https://doi.org/10.1109/EMBC.2015.7319872.

Shichida, Y., and Matsuyama, T. (2009). Evolution of opsins and phototransduction. Philos. Trans. R. Soc. B Biol. Sci. *364*, 2881–2895. https://doi.org/10.1098/rstb.2009.0051.

Sogabe, S. (2017). The Biology of Choanocytes and Choanocyte Chambers and Their Role in the Sponge Stem Cell System. (Doctoral dissertation) (University of Queensland).

Sogabe, S., Hatleberg, W.L., Kocot, K.M., Say, T.E., Stoupin, D., Roper, K.E., Fernandez-Valverde, S.L., Degnan, S.M., and Degnan, B.M. (2019). Pluripotency and the origin of animal multicellularity. Nature *570*, 519–522. https://doi.org/10.1038/s41586-019-1290-4.

Song, H., Hewitt, O.H., and Degnan, S.M. (2021). Arginine Biosynthesis by a Bacterial Symbiont Enables Nitric Oxide Production and Facilitates Larval Settlement in the Marine-Sponge Host. Curr. Biol. *31*, 433–437. https://doi.org/10.1016/j.cub.2020.10.051.

Spafford, J.D., Dunn, T., Smit, A.B., Syed, N.I., Zamponi, G.W., David, J., Dunn, T., Smit, A.B., Syed, N.I., and Zamponi, G.W. (2006). In vitro characterization of L-Type calcium channels and their contribution to firing behavior in invertebrate respiratory neurons. J. Neurophysiol. *95*, 42–52. https://doi.org/10.1152/jn.00658.2005.

Srivastava, M., Simakov, O., Chapman, J., Fahey, B., Gauthier, M.E.A., Mitros, T., Richards, G.S., Conaco, C., Dacre, M., Hellsten, U., et al. (2010). The *Amphimedon queenslandica* genome and the evolution of animal complexity. Nature *466*, 720–726. https://doi.org/10.1038/nature09201.

Svensson, V., Natarajan, K.N., Ly, L.H., Miragaia, R.J., Labalette, C., Macaulay, I.C., Cvejic, A., and Teichmann, S.A. (2017). Power analysis of single-cell RNA-sequencing experiments. Nat. Methods *14*, 381–387. https://doi.org/10.1038/nmeth.4220.

Tsuda, M. (1987). Photoreception and phototransduction in invertebrate photoreceptors. Photochem. Photobiol. *45*, 915–931. https://doi.org/10.1111/j.1751-1097.1987.tb07903.x.

Ueda, N., and Degnan, S.M. (2013). Nitric oxide acts as a positive regulator to induce metamorphosis of the ascidian *Herdmania momus*. PLoS One *8*, e72797. https://doi.org/10.1371/journal.pone.0072797.

Ueda, N., Richards, G.S., Degnan, B.M., Kranz, A., Adamska, M., Croll, R.P., and Degnan, S.M. (2016). An ancient role for nitric oxide in regulating the animal pelagobenthic life cycle: evidence from a marine sponge. Sci. Rep. *6*, 37546–37614. https://doi.org/10.1038/srep37546.

Verasztó, C., Gühmann, M., Jia, H., Rajan, V.B.V., Bezares-Calderón, L.A., Piñeiro-Lopez, C., Randel, N., Shahidi, R., Michiels, N.K., Yokoyama, S., et al. (2018). Ciliary and rhabdomeric photoreceptor-cell circuits form a spectral depth gauge in marine zooplankton. Elife *7*, e36440. https://doi.org/10.7554/elife.36440.

von Salvini-Plawen, L. (2008). Photoreception and the polyphyletic evolution of photoreceptors (with special reference to Mollusca). Am. Malacol. Bull. *26*, 83–100. https://doi.org/10.4003/006.026.0209.

Walter, W., Sánchez-Cabo, F., and Ricote, M. (2015). GOplot: an R package for visually combining expression data with functional analysis: fig. 1. Bioinformatics *31*, 2912–2914. https://doi.org/10.1093/bioinformatics/btv300.

Whelan, N.V., Kocot, K.M., Moroz, L.L., and Halanych, K.M. (2015). Error, signal, and the placement of Ctenophora sister to all other animals. Proc. Natl. Acad. Sci. U.S.A. *112*, 5773–5778. https://doi.org/10.1073/pnas.1503453112.

Wong, E., Mölter, J., Anggono, V., Degnan, S.M., and Degnan, B.M. (2019). Co-expression of synaptic genes in the sponge *Amphimedon queenslandica* uncovers ancient neural submodules. Sci. Rep. *9*, 15781. https://doi.org/10.1038/s41598-019-51282-x.

Yamamoto, H., Tachibana, A., Matsumura, K., and Fusetani, N. (1995). Protein kinase C (PKC) signal transduction system involved in larval metamorphosis of the barnacle, *Balanus amphitrite*. Zoolog. Sci. *12*, 391–396. https://doi.org/10.2108/zsj.12.391.

Yan, Y., and Wagner, F. (2018). Generate the UMI count matrix from CEL-Seq2 sequencing data. https://github.com/yanailab/celseq2.

Yarfitz, S., and Hurley, J. (1994). Transduction mechanisms of vertebrate and invertebrate photoreceptors. J. Biol. Chem. *269*, 14329–14332. https://doi.org/10.1016/s0021-9258(17)36620-6.

Yule, D.I., and Williams, J.A. (1992). U73122 inhibits Ca2+ oscillations in response to cholecystokinin and carbachol but not to JMV-180 in rat pancreatic acinar cells. J. Biol. Chem. *267*, 13830–13835. https://doi.org/10.1016/s0021-9258(19)49643-9.

STAR★METHODS

KEY RESOURCES TABLE

REAGENT or RESOURCE	SOURCE	IDENTIFIER
Biological samples		
Adult *Amphimedon queenslandica* used for larval release	Heron Island Reef Great Barrier Reef	N/A (perished or returned to reef)
Chemicals, peptides, and recombinant proteins		
salt for UQ aquaria	Tropic Marin®	Pro-Reef Sea Salt
2-APB (2-aminoethoxydiphenyl borate)	Sigma-Aldrich	D9754
2-OH-saclofen (2-hydroxy-saclofen)	Sigma-Aldrich	A6566
AP3 (L-(+)-2-amino-3-phosphonopropionic acid)	Sigma-Aldrich	A154
cGMP (guanosine 3′,5′-cyclic monophosphate sodium)	Sigma-Aldrich	G6129
CM-DiI	ThermoFisher	C7000
DMSO (dimethyl sulfoxide)	Sigma-Aldrich	D8418
DMSO (dimethyl sulfoxide) - sterile	Sigma-Aldrich	D2650
Fura Red	ThermoFisher	F3021
GABA (γ-aminobutyric acid)	Sigma-Aldrich	A5835
L-glutamic acid	Sigma-Aldrich	G1251
L-NAME (N_ω-Nitro-L-arginine methyl ester hydrochloride)	Cayman Chemical	80210
Neutral Red	ProSciTech	C127
nifedipine	Abcam	Ab120135
pluronic acid F-127	ThermoFisher	P3000MP
PTIO (α-phenyltetramethylnitronyl nitroxide)	Sigma-Aldrich	P5084
staurosporine	Sigma-Aldrich	S4400
TPA (phorbol-12-myristate-13-acetate)	Cell Signalling	4174
U-73122	Sigma-Aldrich	U6756
Reagents for CEL-Seq2 library	(Hashimshony et al., 2016)	N/A
Deposited data		
CEL-Seq2 raw reads	NCBI Sequence Read Archive	NCBI SRA: SRR13695362
CEL-Seq2 mapped-gene counts	Github	https://github.com/AquSensory/Phototransduction2020
Software and algorithms		
R code for differential expression analyses	Github	https://github.com/AquSensory/Phototransduction2020
CEL-Seq2 analysis pipeline	(Yan and Wagner, 2018)	N/A

RESOURCE AVAILABILITY

Lead contact

Further information and requests for resources and reagents should be directed to and will be fulfilled by the lead contact, Bernard Degnan (b.degnan@uq.edu.au).

Materials availability

This study did not generate any unique materials.

Data and code availability

- CEL-Seq2 raw reads have been deposited on NCBI Sequence Read Archive. Accession number is listed in the key resources table.

- All original code has been deposited on Github and is publicly available as of the date of publication. DOIs are listed in the key resources table.
- Any additional information required to reanalyze the data reported in this paper is available from the lead contact upon request.

EXPERIMENTAL MODEL AND SUBJECT DETAILS

Animals

Adult *Amphimedon queenslandica* were collected from shallow intertidal reef flats at Shark Bay, Heron Island Reef under Great Barrier Reef Marine Park Authority permit G16/38120.1. For phototaxis assays, larvae were obtained from animals maintained in outdoor aquaria with flow-through, unfiltered, ambient seawater at the Heron Island Research Station. For single cell sequencing, larvae were obtained from animals transported to the University of Queensland (UQ) aquaria. Animals were subjected to mild heat shock of 1–2°C to induce larvae release from adults. Upon emergence, larvae were collected with a disposable pipette and transferred to 0.22 μm-filtered seawater (FSW).

METHOD DETAILS

Isolation of larval cell types for CEL-Seq2

Larval cells were isolated by dissociating each larva in approximately 20 μL FSW with tituration through a 200 μL pipette tip. Each dissociated larva in FSW was diluted to approximately 500 μL in FSW to reduce cell density and thus allow for optimal cell identification and isolation under a microscope. Dissociated cells were kept in an ice-water bath for the duration of cell harvest.

Using Differential Interference Contrast (DIC) and epifluorescence on a Nikon Eclipse Ti inverted microscope, dissociated larval cells were identified by size and shape and by differential dye uptake. The lipophilic fluorescent dye CM-DiI (CellTracker) differentially labelled flask cells when larvae were incubated in 1 μM for <1 h) (Nakanishi et al., 2014, 2015). The lysosomal dye Neutral Red differentially labelled globular cells (fluorescent red at 2 μM) and cuboidal cells (bright red at 10 μM) (Figure 1).

Selected cells were isolated using a Nikon Narashige NT-88-V3 micromanipulator driven by an Eppendorf CellTram Vario. The micromanipulator was fitted with a borosilicate glass capillary (OD 1 mm, ID 0.78 mm) pulled by a Sutter Instrument P-97 flaming/ brown micropipette puller. Capillary tips were opened by gently stabbing through a taut piece of Kimwipe. Cells were collected in 0.5–1 μL FSW, placed in 0.2 mL Eppendorf tubes and snap-frozen in an ethanol-dry ice bath before being stored at −80°C. Eight samples were collected for each of the seven cell types. Details on parent sponge and number of cells in each collection pool are recorded in Table S1.

CEL-Seq2

Cell samples were pooled and two DNA libraries were constructed (Table S1) as per the CEL- Seq2 protocol (Hashimshony et al., 2016). Library 1 was sequenced as two runs on the Illumina NextSeq500 platform at the University of New South Wales Ramaciotti Centre for Genomics. For the first run, an entire flow cell (comprising four interconnected lanes) was used and the library was loaded at the standard concentration of 11 pM, with 15% PhiX spike-in to overcome low base diversity due to the presence of CEL-Seq barcodes. Customized paired-end reads were performed (R1: 15 bp covering sample-specific barcodes and the Universal Molecular Identifiers (UMI); R2: 55 bp covering mRNA transcripts), with no index reads. A second sequencing run was performed on the same library under the same run configurations, except with a lower loading concentration (8 pM) and higher (20%) PhiX spike-in. Library 2 was sequenced on the Illumina HiSeq4000 platform at the Brisbane node of the Australian Genome Research Facility (AGRF). For this run, the library was loaded at 8 pM in one lane with 20% PhiX spike-in, and read with the standard paired-end format of 75 bp × 2.

CEL-Seq2 analysis pipeline

Raw sequencing reads were filtered for low base-calling quality (R2 average Phred score < 30; presence of "N" in a read) and assessed for adaptor contents using FastP (Chen et al., 2018). Filtered reads were then demultiplexed and mapped to the *Amphimedon* Aqu2.1 genome (Fernandez-Valverde et al., 2015) following the CEL-Seq2 Python analysis framework (Yan and Wagner, 2018), generating transcript counts of each gene for each cell sample. Using recommended filtering parameters for scRNA-Seq

(Grün and Van Oudenaarden, 2015), samples with total reads < 1 million, mapped transcripts < 0.5 million, ERCC to sponge transcript ratio > 0.1 (indicating low sponge input material), and mapping success of < 25% were discarded (Table S1). These cut-off values followed previous determinations of sequencing depth and mapping rates of CEL-Seq2 data on *Amphimedon* adult single cells (Sogabe et al., 2019; Svensson et al., 2017). Principal component analysis (PCA) was performed in R on variance-stabilizing-transformed (vst) counts (DESeq2) to visualize transcript abundance across cell types; samples appearing as significant outliers were used to re-evaluate the cut-off values for filtering.

Gene function analysis

Over a genome-wide Blast2Go (Conesa et al., 2005) scan, each Aqu2.1 gene was annotated with a description based on BLAST sequence similarity and with associated gene ontology (GO) terms based on InterProScan (Jones et al., 2014) results. For specific genes of interest (cryptochrome (CRY), metabotropic glutamate receptors (mGluR), γ-aminobutyric acid receptors (GABAR), inositol triphosphate receptor (IP3R), nitric oxide synthase (NOS), protein kinase C (PKC) and voltage-gated calcium channel (VGCC), *Amphimedon* paralogues or orthologues were designated based on further information including conserved domains (Wong et al., 2019) and pre-existing functional and phylogenetic analyses (Bettler et al., 2004; Krishnan et al., 2014; Moran et al., 2015; Rivera et al., 2012; Senatore et al., 2016).

For this study, a gene is considered "neural" if (i) it is a synaptic gene (Wong et al., 2019); (ii) it is one of the 27 identified *Amphimedon* homeobox genes (Sogabe, 2017); or (iii) if either its description or (iv) its associated GO terms includes neural descriptors, i.e. with at least one of the following keywords: synap*, neuro*, neura*, nerv*, brain, cerebell*, cerebr*, axon*, dendri*, myosin, cell body, memory, learning (* stands for wildcard). Enrichment tests were determined against background levels in Aqu2.1 protein coding genes, using Fisher's Exact test implemented in R. Across DEGs in each cell type, the top five most enriched GO terms for both Biological Process and Molecular Function were identified. The relationships between DEGs and GO terms of interest are presented using R package GOplot (Walter et al., 2015). Z-scores of GO terms were calculated by:

$$\frac{(\text{number of upregulated genes} - \text{number of downregulated genes})}{\sqrt{\text{number of DEGs assigned to this term}}}$$

Domain analysis

To identify domain composition of cell types and genes of interest, peptide sequences were submitted to the Pfam website (Finn et al., 2016) via "Batch sequence search" against the Pfam-A seed alignment curation database; threshold was set at $1e^{-03}$. DEGs (p-adj< 0.05) of selected cell types were contrasted on domain gene occurrence (number of genes a domain appears in, regardless of repetitive domains); percentages were taken against the total number of DEGs.

Phototaxis assays

Setup

A transparent chamber (7.5 × 2.2 × 1.3 cm) filled with 20 mL FSW was used for all assays. To create a light gradient along the chamber, a white light source (Olympus LG-PS2, at maximum output) was placed at one end behind a layer of light diffuser sheet, and black filter paper was used to cover the external wall of the chamber on the other end (Figure 3A). Light intensity, as measured by a LI-COR LI-190R Quantum Sensor / LI-1400 data logger, was 950 μM photons $m^{-2}s^{-1}$ at the edge of the chamber towards the bright end and 80 μM photons $m^{-2}s^{-1}$ towards the dark end; these are within an ecologically relevant spectrum representing light intensities on a sunny day on an exposed part of the reef flat and under coral rubble, respectively (Leys and Degnan, 2001).

Controls

Newly emerged larvae were allowed to acclimate to room temperature (25°C) for 30 min. To document normal larvae phototactic behaviour, 10 larvae between the age of 2–3 hpe were loaded into the bright end of the chamber using a pipette (Figure 3A). A compact digital camera (Olympus Tough TG-4) held with a retort stand recorded larvae movement from above at 30 frames per sec (fps) for just over one minute. The video was then scored for the number of larvae appearing in each quartile of the chamber (Q1 to Q4 from bright end to dark end) at every five-sec interval for a total of one minute. Each assay was replicated three times with a new set of 10 larvae each time.

Treatments

We tested the effect on larvae phototaxis of 13 agonists and antagonists of opsin-based phototransduction pathway proteins. These selections, as well as working concentrations and pre- incubation time, were determined based on previous results on marine invertebrate physiology (Table 1; (Chrachri et al., 2005; Conn et al., 2018; DeRiemer et al., 1985; Ebanks et al., 2010; Ellwanger et al., 2007; Ellwanger and Nickel, 2006; Fulton et al., 2008; Galione et al., 1993; Matzel et al., 1995; Nagy and Contzen, 1997; Okazaki and Shizuri, 2000; Parnas et al., 1999; Spafford et al., 2006; Ueda et al., 2016; Ueda and Degnan, 2013; Yamamoto et al., 1995). To ensure that a reagent did not alter larval mobility, ten larvae were incubated in each reagent at 0.5, 1, 2 and 5 times the published effective concentrations and observed against those of the control (FSW or with equivalent volume of DMSO) for 24 hours. The highest concentration where no mortalities nor mobility issues was observed was adopted as the optimal working concentration. Each reagent was added to FSW in the chamber from stock volumes and larvae were pre-incubated immediately prior to the experiment as necessary (Table 1). Larval phototactic behaviour was recorded in the same manner as described for untreated controls, with three replicates for each treatment.

Combination Treatments

Based on results of treatments, phototaxis assays were performed on combinations of two reagents with opposing effects to establish the order of their effects in the signalling cascade. Both reagents were loaded into FSW in the experiment chamber at optimal concentrations and larvae were pre-incubated with both reagents simultaneously as required.

QUANTIFICATION AND STATISTICAL ANALYSIS

Differential gene expression analysis

Differential gene expression analysis was performed using Wald test implemented in DESeq2 (Love et al., 2014) at the significance level of p-adj< 0.1 (DESeq2 default). To improve the detection of differentially expressed genes (DEGs) (Sha et al., 2015), genes with overall transcript counts of less than 10 across all 24 samples were removed, then the 25% of remaining genes that had the lowest variance were also removed from analyses. DEGs were extracted using two approaches: (i) expression level is contrasted groupwise (e.g. epithelial vs non-epithelial cells), and (ii) by all possible pairwise comparisons. These data were presented using GraphPad Prism (v 8.1.0) and the R package Upset (Conway et al., 2017) respectively.

Phototaxis assay analysis

Negative phototaxis was manifested in the experimental setup as a decreasing number of larvae in Q1 and an increasing number of larvae in Q4 over time, hence Q1 and Q4 series raw counts (Table S3) were contrasted for treatments of interest. The linear mixed effects model (lme) was implemented using the R package lme4 (Bates et al., 2015) to model larvae counts with and without the treatment effect for the Q1 series and the Q4 series separately. The difference between the models were then assessed with the likelihood ratio test. Normality and variance of residuals were checked with QQ and residual plots, respectively. Stacked bar graphs were used to visualise distributions of larvae over the four quartiles, averaging three replicates for each treatment; errors bars were not shown due to overlap. Graphs were generated and statistical analyses were performed in GraphPad Prism 8 and R Studio, respectively.